Nature of the Atmospheric Dynamics on Venus from Power Spectrum Analysis of Mariner 10 Images

LARRY D. TRAVIS

Goddard Institute for Space Studies, NASA, New York, NY 10025

(Manuscript received 6 March 1978, in final form 3 May 1978)

ABSTRACT

Mariner 10 Venus images are analyzed into power spectra of the brightness field for planetary zonal wavenumbers $n \geq 3$ and for latitudes from 55°S–25°N. These spectra are examined for significant features and latitudinal variation as well as compared with cloud brightness distribution spectra similarly determined for the Earth. The Venus image spectra are found to have a systematic variation as a function of latitude. In the equatorial region the average power spectrum has an approximately -2.7 power law behavior for $n > 5$, while in midlatitudes the average spectrum is characterized by a slope of about -1.8 for $n \geq 3$. Although a flattening of the equatorial region spectrum for wavenumbers less than 5 is noted, no obvious peaks are superimposed on the general power law behavior of the Venus spectra. This is in contrast to the result for the Earth cloud brightness spectra, which exhibit a noticeable peak near wavenumber 5 or 6 for the midlatitude region.

The Venus image spectra are further interpreted under the assumption that the UV cloud features serve as markers of large-scale dynamical processes and thus can reveal the characteristics of the eddy kinetic energy spectrum. Support for this assumption is provided by the results of a comparison of the cloud brightness spectra for the Earth with observed eddy kinetic energy spectra. The characteristics of the Venus spectra at low latitudes suggest that the observed clouds are in a region of high static stability in which the large-scale turbulence is essentially two-dimensional, and that the important energy sources are at the largest scales ($n < 5$), with the spectrum exhibiting a slope close to the theoretically expected -3 value for an inertial subrange at larger wavenumbers. It is concluded that the less steep slope observed for the midlatitude spectrum is quite possibly the manifestation of the importance of barotropic eddy disturbances in that region.

1. Introduction

The dominant feature of the dynamical state of the upper troposphere and lower stratosphere of Venus is the apparent strong zonal circulation with typical velocities of 90 m s^{-1}. This surprising state was first suggested by ground-based observations of the dark markings in the ultraviolet, which exhibit a retrograde rotation with a period on the order of 4 days, corresponding to equatorial speeds of about 110 m s^{-1} (Boyer and Camichel, 1961; Smith, 1967; Boyer and Guerin, 1969; Scott and Reese, 1972). Using the higher resolution afforded by the Mariner 10 images, Suomi (1975) has derived cloud-tracked winds for the small scale UV clouds and finds velocities on the order of 90 m s^{-1} in the equatorial region, a possible increase to slightly more than 100 m s^{-1} near latitude 40°, and a decrease at higher latitudes to an apparently constant angular velocity. These cloud-tracked wind vectors show relatively little, if any, meridional motion.

Because of the nearly complete lack of information on the substance causing the UV absorption, observations of the apparent motion of such features provide no means to distinguish between a wave phenomenon or actual mass motions. Evidence that there are in fact retrograde zonal mass motions on the order of 100 m s^{-1} in the upper atmosphere has come from spectroscopic observations of molecular absorption lines formed at altitudes 50–80 km in the atmosphere of Venus and from analysis of the Doppler shifts of the telemetry signals from Venera 7–10 spacecraft. The CO_2 line shift observations carried out by Traub and Carleton (1975) yield a mean zonal wind velocity near the equator of 83 ± 10 m s^{-1} in the retrograde sense and a weak meridional velocity on the same order as the measurement errors. Analyses of the Venera 7–10 data (Marov *et al.*, 1973; Ainsworth and Herman, 1975, 1977; Antsibor *et al.*, 1976; Kerzhanovich and Marov, 1977) result in implied zonal velocities in the range of 60 to 150 m s^{-1} at 50 km altitudes. Although reduced in magnitude below 40 km, the velocities may be 10–20 m s^{-1} at altitudes as low as 15 km. Thus, the zonal circulation appears to indeed represent actual mass motion and extends throughout a substantial part of the atmosphere.

Wave phenomena superimposed on this basic circulation are of course not precluded. In fact, based on the

assumption that the velocities obtained by Suomi (1975) for small UV features reflect the true physical displacements, Belton *et al.* (1976a,b) argue that the persistence and morphology of the large, horizontal Y feature can be explained only by planetary-scale waves propagating relative to these winds.

The evidence thus far gives no obvious indication of whether the meridional circulation or the large-scale eddies in the zonal circulation play the dominant role in meridional transport of momentum and energy. The details of the kinetic energy spectrum for the eddies should provide information on the scale of maximum instability and the conditions governing the mechanism of interaction between various scales. An indication of the importance of eddies relative to the mean meridional circulation should also be valuable for helping to identify and understand the driving mechanism for the strong zonal winds.

While a direct specification of the eddy spectra utilizing cloud-tracked winds from Mariner 10 images would be desirable, such an approach is probably not feasible because of typical errors of 5–10 m s^{-1} for an individual velocity determination. Large velocity variances over large spatial scales might be discernible, but obtaining information on scales with planetary wavenumber greater than about 4 or 5 in this manner is unlikely. However, an indirect approach employing power spectrum analysis of the cloud brightness distribution offers a potential alternative. Chang (1970) and Wallace (1970) have demonstrated that time-longitude displays of Earth satellite cloud brightness data can be used to clearly show westward propagating cloud systems in the tropical Pacific. The correlation of such cloud bands with independent wind field measurements has established that propagating waves can indeed be observed in this manner (Wallace, 1971; Reed and Recker, 1971). Consequently, the use of time and spatial spectrum analysis of satellite-observed brightness in order to examine the scales of tropical wave disturbances has become a relatively common practice (Tanaka and Ryuguji, 1971, 1973; Sikdar *et al.*, 1972; Young and Sikdar, 1973; Gruber, 1974; Zangvil, 1975). Although these studies have been restricted to transient eddy phenomena in the tropics, the possibility of employing such a technique to investigate the spatial spectrum of eddies on a global basis is certainly suggested.

The purpose of this paper is to present the results of power spectrum analyses on a set of Mariner 10 Venus images and to examine these spectra for significant features as well as variation with latitude. In addition, we compare the Venus image spectra with cloud brightness distribution spectra for the Earth determined in the same manner. Further interpretation of the Venus spectra is made on the basis of the assumption that the cloud features respond to large-scale dynamical processes and therefore can provide information on the characteristics of the eddy kinetic energy spectrum. The validity of this assumption for the terrestrial case is examined by comparing observed eddy kinetic energy spectra with cloud brightness distribution spectra for the Earth. Although the extension of this assumption to the situation for Venus could prove to be misleading in view of our lack of information on the physical processes associated with the UV cloud features, the resulting interpretation of the Venus spectra may provide important insights on the role of eddies.

In the next section the power spectra obtained from the Venus images are shown, preceded by a description of the method of analysis employed. This is followed in Section 3 by a comparison between the results of similar calculations for Earth images and observed eddy kinetic energy spectra. Section 4 is a discussion of the implications of the Venus spectra, and Section 5 is a brief summary of the conclusions.

2. Power spectra of Venus images

The numerous images returned from the Mariner 10 Venus encounter have provided the first high resolution view of the UV cloud patterns, showing a wealth of interesting detail (Murray *et al.*, 1974; Belton *et al.*, 1976a). The Image Processing Laboratory of the Jet Propulsion Laboratory has kindly provided us with a number of these images in which the complete disk of the planet is within the field of view of the vidicon camera, and for which geometric and photometric distortions have been removed. Thus, the basic image data consists of 8-bit data numbers representing the intensity of each pixel, with the Venus disk diameter approximately 500 pixels. In the present study, power spectrum analysis has been performed on eight images; these are identified in Table 1 by the Flight Data System (FDS) number along with the pertinent information on each image.

Before spectrum analysis of the cloud brightness distribution is carried out, it is desirable to first remove the effect of the variation in brightness across the disk due to differing scattering geometry. The procedure that we have adopted involves the calculation of the theoretical intensity as a function of position on the disk for a horizontally homogeneous atmosphere which has a spherical albedo of 0.55 at 0.355 μm, the effective wavelength of the Mariner 10 UV imaging filter.[1] A single type of cloud particle with the vertical distribution derived by Lacis (1975) is assumed to represent the observable cloud deck. The optical scattering characteristics of the cloud particles are those specified by the interpretation by Hansen and Hovenier (1974) of polarization observations.[2]

[1] This spherical albedo is taken from the analysis by Travis (1975) of the ground-based photometry of Venus carried out by Irvine *et al.* (1968a,b).

[2] Although the identification of these particles as concentrated sulfuric acid droplets leaves the ultraviolet absorption unex-

TABLE 1. Mariner 10 Venus images.

Identification no.	Date	Time (GMT)	Range (km)	Resolution*	Sub-spacecraft point** Latitude (°S)	Sub-spacecraft point** Longitude (deg)	Phase angle (deg)
FDS 63903	8 Feb 74	1613	2 118 638	47	18.80	219.64	28.4
FDS 64117	8 Feb 74	1843	2 192 546	49	18.80	219.81	28.3
FDS 64747	9 Feb 74	0204	2 410 250	53	18.79	220.28	27.9
FDS 64897	9 Feb 74	0349	2 462 113	55	18.79	220.40	27.8
FDS 65179	9 Feb 74	0707	2 559 637	57	18.79	220.60	27.6
FDS 65473	9 Feb 74	1032	2 661 374	59	18.79	220.82	27.5
FDS 66223	9 Feb 74	1917	2 921 155	65	18.78	221.37	27.0
FDS 66385	9 Feb 74	2111	2 977 319	66	18.77	221.48	26.9

* Resolution at the sub-spacecraft point.
** Latitude and longitude in the IAU Venus coordinate system.

For this model, the theoretical intensity as a function of observer zenith angle and solar zenith angle is obtained using the fast invariant imbedding numerical method for multiply-scattering atmospheres developed by Sato *et al.* (1977). The specification of such a theoretical intensity corresponding to each pixel in an image required first a "navigation" of that image, i.e., knowledge of the planetary coordinates of each pixel and the location of the subsolar point. This navigation is uniquely defined from the known IAU Venus coordinates for the sub-spacecraft and sub-solar points, the location of the pixel corresponding to the center of the disk, and the fact that the nominal orientation of three-axis stabilized Mariner spacecraft was such that the sub-spacecraft and sub-solar points are on the same scan line. Then, at each pixel in the image, the appropriate theoretical intensity is normalized to a value which can be compared to the observed data number by means of the ratio of the respective disk-integrated intensities. By subtracting these normalized intensities from the observed data numbers, we are left with a brightness distribution corresponding only to intrinsic variation in the clouds, with negative values for darker than average regions and positive values for the lighter features.

In order to facilitate meaningful comparisons between the results of analyses for different images, a mapping of intensity levels to obtain a new image with an equalized intensity histogram of 10 levels is performed in each case. The typical intensity histogram for Venus images corrected for the scattering geometry variation is relatively sharply peaked, with a half-width of about 15 data numbers. Thus, histogram equalization converts the finely quantized image which has a distribution largely restricted to a narrow range of intensity levels into one of fewer levels but with enhanced contrast discrimination for the most frequently occurring intensities. The choice of 10 levels for the transformed image is based on the narrowness of the original histogram peak and the fact that the mode intensity level includes approximately 7% of the pixels in the disk. In view of the substantial difference in the appearance of Earth and Venus images, the normalization provided by such histogram equalization is probably a prerequisite for a valid comparison. However, power spectra obtained with and without the use of this procedure are examined to establish the extent of its effects.

Using the "navigation" of the images described previously, it is a simple matter to tabulate the intensity variation along latitude circles for analysis of the zonal spectrum. This is carried out for latitudes in steps of 1° from 55°S to 25°N, the limits of this range being chosen to avoid large foreshortening effects. Intensities at five points per degree of longitude along the visible portion of each latitude circle are obtained by means of bilinear interpolation between the values for the four pixels nearest the point in question. Since the phase angle for the images under consideration is about 28°, intensities for approximately 150° in longitude, or 750 points, can be tabulated for the typical latitude circle. In practice, this is further reduced to ~650 points by the elimination of the poorly defined, foreshortened region near the limb. Thus, the basic data are capable of yielding information for zonal wavenumbers of 3 and larger.

Before performing the spectrum analysis we smooth the intensity data for each latitude, using a modified normal curve smoothing function. The smoothed intensity $\bar{I}_N$ at the Nth point is therefore

$$\bar{I}_N = \sum_{m=-15}^{15} W_m I_{N+m},$$

where the weights W_m are specified by

$$W_m = C \exp(-m^2/2\sigma^2),$$

with σ set at 10 and C chosen to normalize the sum of

plained, we have simply chosen that small imaginary part for the index of refraction necessary to obtain the desired spherical albedo with this model. The effect of this assumption on the theoretical intensity distribution, as compared to other plausible procedures for distributing the requisite absorption, is insignificant.

the weights.[3] The purpose of this procedure is to eliminate low wavenumber aliasing caused by the high frequencies corresponding to the relatively sharp edges of the clouds in Earth images. Although this effect should be small for the Venus images, the smoothing is applied to all intensity data in order to keep the method of analysis as similar as possible for the two planets. This smoothing limits high-frequency resolution to planetary wavenumbers $\lesssim 30$.

The power spectrum for each latitude is obtained in a standard manner, taking the Fourier transform of the autocorrelation function. Since there is of course intensity data only for a portion of each latitude circle, the specification of the power for integral planetary zonal wavenumbers in general requires evaluation of the transform using nonintegral wavenumbers relative to that fraction of the latitude circle for which there is data. Thus, for example, the minimum *planetary* zonal wavenumber on which information is provided by analysis of data covering 40% of a latitude circle is 2.5, and that is obtained using $n = 1$ relative to the actual span of the data. To obtain the power at the integral planetary wavenumber 3, we must perform the transform for $n=1.2$. This procedure is in fact mathematically equivalent to setting the data corresponding to the unobserved portion of the latitude circle equal to zero and performing the analysis for the complete 360° using only integral wavenumbers. It is therefore important that the mean value over the observed portion be subtracted from that intensity data before spectrum analysis is performed, since this insures that no spurious power is generated due to a fraction of the latitude circle having a higher average than the remaining points all set at zero. Although it is perhaps natural to question whether this procedure may not introduce a bias into the spectral analysis, we performed experiments with artificial data of known power spectra, and these indicate that little distortion should exist for wavelengths smaller than that corresponding to the data span. Furthermore, calculations by Julian *et al.* (1970) of terrestrial atmospheric kinetic energy spectra using observed winds over only 180° in longitude showed very close agreement for wavenumbers 2 and larger with results using data over the full 360°.

As may be expected for most spectrum analyses, the results for a single latitude for a particular Venus image appear relatively noisy, showing minor peaks of no statistical significance. An examination of the data for all eight images does reveal, however, a discernible latitudinal variation in the general characteristics of the power spectra. Consequently, we have selected three latitude zones over which an average power

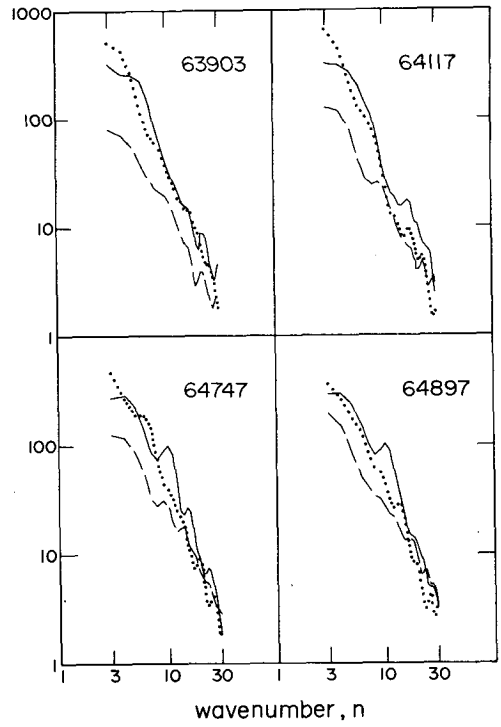

FIG. 1. The individual cloud brightness power spectra for Mariner 10 Venus images: FDS 63903, 64117, 64747 and 64897. The equatorial region (15°N–15°S) is represented by the solid line, the midlatitude zone (35–55°S) by the broken line, and the intermediate region (15–35°S) by the dotted line. The absolute value of the power is arbitrary, being simply a function of the normalized intensity scale of the image.

spectrum is computed for each image.[4] These zones are 15°N–15°S, 15–35°S and 35–55°S. This choice reflects not only the objective of displaying the difference between the equatorial and midlatitude regions, but also the preference for symmetry with respect to the equator for the first zone and sufficient width for each zone so that the average is statistically meaningful. The resulting average power spectra for the eight Venus images are displayed in Figs. 1 and 2, with the solid line representing the 15°N–15°S zone, the dotted line 15–35°S, and the broken line 35–55°S, and where of course the lines connect the respective values at the discrete wavenumbers from 3–30. The units of power on the ordinate are arbitrary, simply reflecting the choice of a 10-level intensity scale for the histogram equalized images.

Although a certain amount of noise in the form of spurious peaks remains in spite of the averaging, a systematic difference between the equatorial zone and the midlatitude region is clearly evident. The overall slope of the decrease in power with increasing wavenumber is obviously less steep for the 35–55°S zone than

[3] This normal curve smoothing was chosen in order to avoid the undesirable frequency response of equally weighted running means (Holloway, 1958); however, a comparison with such running means showed insignificant differences for the present application.

[4] For this and all other averaging processes, logarithmic averaging is employed in order to place the emphasis on the shape of the spectrum rather than on the absolute magnitude of the power at a particular wavenumber.

for the equatorial region. On the other hand, there is a noticeable flattening of the power spectrum near wavenumbers 3–5 for the 15°N–15°S zone, with relatively little such tendency apparent for the other zones. The spectrum for the intermediate zone generally falls between the other two, both in magnitude and slope. However, since it shows no tendency for flattening at the lowest wavenumbers, it crosses the spectrum for the equatorial regions near wavenumber 3 or 4 for most images.

The eight Venus images cover a time span of about 29 h, during which the high zonal winds presumably carried any long-lived cloud features through 80–100 degrees in longitude. Since the sub-spacecraft point changed by less than 2° during this period, the images at the beginning and end of the sequence can be expected to show significantly different cloud patterns. Also, many smaller features may have lifetimes no greater than a few hours (Murray *et al.*, 1974). The relative similarity of the power spectra for the pairs separated by less than 2 h, FDS 64747 and 64897, 66223 and 66385, may in fact illustrate the time scale over which no major changes occur. Images separated by much longer time intervals yield power spectra with readily apparent differences, but the general characteristics detailed above are maintained.

Power spectra for the three latitude zones averaged over all eight images are displayed in Fig. 3. This averaging removes most of the noise peaks appearing in the individual spectra, leaving the apparently

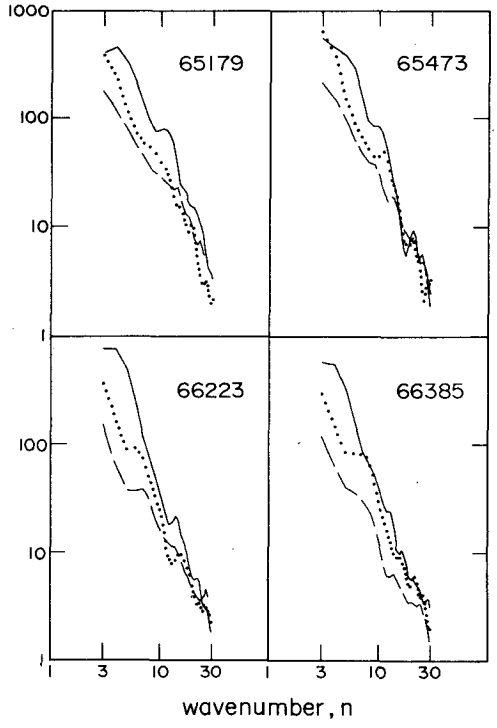

FIG. 2. As in Fig. 1 except for images FDS 65179, 65473, 66223 and 66385.

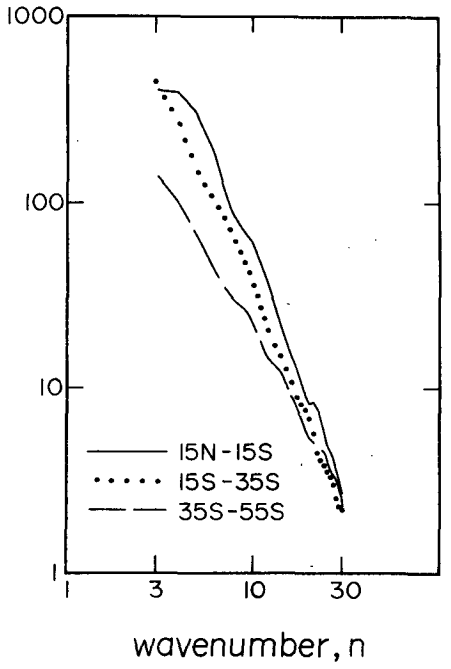

FIG. 3. Venus cloud brightness spectra for the indicated latitude zones, averaged over all eight Mariner 10 images analyzed.

statistically significant features already suggested. It also becomes somewhat easier to characterize the slopes of the power spectra quantitatively. Visual linear fits between wavenumbers 3 and 20 yield a slope of −1.7 for the midlatitude region, −2.3 for the 15–35°S zone, and between wavenumbers 5 and 20, a value of −2.7 for the equatorial region. If the power spectra are averaged over all latitudes from 25°N–55°S and for the complete set of eight images, we find a slope of −2.3 between wavenumbers 5 and 20, and approximately −1.2 between wavenumbers 3 and 5.

When the identical analysis is applied to images for which histogram equalization has not been performed, a somewhat greater variability between the power spectra for different images is noted. The same basic characteristics are retained, but quantitatively modified somewhat for the intermediate and midlatitude zones. Inspection of the power spectra averaged over the eight images then suggests a slope of −2.0 for 35–55°S and −2.2 for 15–35°S, with their respective spectra nearly equal in magnitude as well as slope. The shape and the slope of about −2.7 of the spectrum for the equatorial region is essentially unchanged, and the magnitude of the power at low wavenumbers remains greater than that for the midlatitude region. These differences perhaps serve as an indication of the degree of uncertainty which should be taken into consideration in any interpretation of the power spectra. In any event, the evidence for a significant difference between the equatorial and midlatitude regions seems clear.

TABLE 2. Earth images.

Spacecraft/ID	Date	Time (GMT)	Resolution* (km)	Sub-spacecraft point Latitude (deg)	Sub-spacecraft point Longitude (deg)	Phase** angle (deg)
Mariner 10 FDS 14553	10 Nov 73	0151	58	4.3°N	121.1°W	92
SMS-1	16 Jul 74	1830	10	~0	~45°W	54
SMS-1	1 Aug 74	1800	10	1.6°S	44.6°W	47
SMS-1	17 Aug 74	1800	10	~0	~45°W	46
SMS-1	2 Sep 74	1830	10	0.7°N	45.4°W	52
SMS-1	27 Sep 74	1830	10	~0	~45°W	55
GOES-1	5 Jun 76	1700	19	~0	~75°W	23

* Resolution at the sub-spacecraft point.

** Phase angle for the sub-spacecraft point only. The SMS-1 and GOES-1 satellites are at an altitude of approximately 35 800 km; therefore, the phase angle for a particular point can differ from the indicated value by as much as 10°. The Mariner 10 spacecraft was at a range of about 2 600 000 km when FDS 14553 was acquired, so the phase angle varies by less than 0.14° from that at disk center.

3. Comparison of Earth image power spectra with kinetic energy spectra

The same type of analysis used on the Mariner 10 Venus image data has also been applied to a set of Earth images. This consists of one Mariner 10 image made with the orange filter ($\lambda_{eff}=0.578$ μm), five pairs of visible (0.55–0.75 μm) and thermal IR (10.5–12.6 μm) images from SMS-1, and one such pair from GOES-1. The dates and times of image acquisition are given in Table 2, along with other pertinent information. All SMS and GOES data are partial disk images, with coverage from 10–58°N for the GOES image, and 20°S–70°N for all SMS images except 16 July 1974 which is 20°S–60°N. The Mariner 10 image allows data to be obtained from 50°S to approximately 60°N.

Since the thermal IR images are reversed in the sense that higher intensity levels correspond to lower temperatures, the colder cloud tops are the dominant feature, allowing these images to be viewed in much the same way as their counterparts in the visible. Actually, in the present application we have analyzed the IR images alone as well as composites formed from linear combination of the visible and IR images. The purpose in generating such composite images is an attempt to suppress the differences in intensity between land and ocean not covered by clouds. This can be effected reasonably well for the Northern Hemisphere summer regions under consideration because the warmer land is darker than the ocean in the thermal IR images, while the albedo of the land in the visible is higher than that of the ocean. For most regions where there are clouds, however, both images are bright, and there is reinforcement. There is of course some discrimination between the two types of images since the thermal IR images tend to emphasize the colder, and therefore higher, clouds.

As with the Venus image power spectra, calculations are performed for latitudes in steps of 1°, and these results are then averaged over zones in order to eliminate some of the statistical fluctuations. Most available eddy kinetic energy spectra have been obtained from data for midlatitude regions. Consequently, one of the zones that we have selected covers latitudes from 25–65°N, except for the GOES and 16 July SMS images, which are limited to 58 and 60°N, respectively. For the Mariner 10 image from November, the corresponding region was taken as 25–50°S in order to examine the summer hemisphere for all images. Despite the paucity of eddy kinetic energy data for the tropics, there are indications that this region exhibits interesting contrasts from the situation at midlatitudes. Thus, we have also examined the zone from 15°N–15°S.

The resulting Earth image power spectra are shown in Fig. 4a for the midlatitude zone and Fig. 4b for the equatorial region. The solid line corresponds to the spectrum for the Mariner 10 image, the dotted-broken line for the GOES image, the dotted line for the average of the 5 SMS visible/IR composites, and the dashed

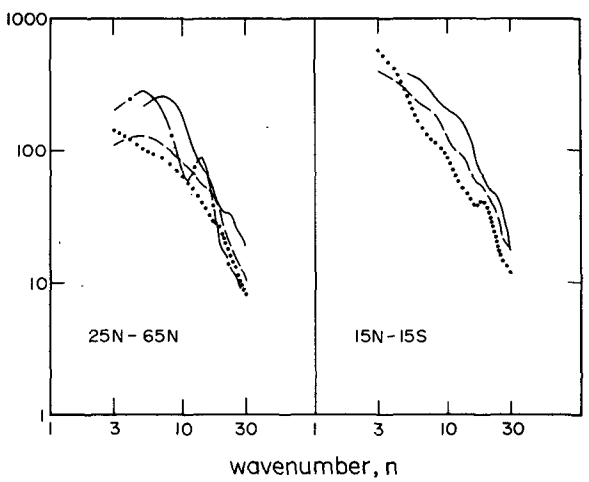

FIG. 4. Earth cloud brightness power spectra from a Mariner 10 image (solid line), a GOES image (dotted-broken line), an average of five SMS visible/IR composites (dotted line) and an average of the five SMS thermal IR images (dashed line). Part (a) shows the results for a midlatitude zone (25–65°N), and part (b) represents the equatorial region (15°N–15°S).

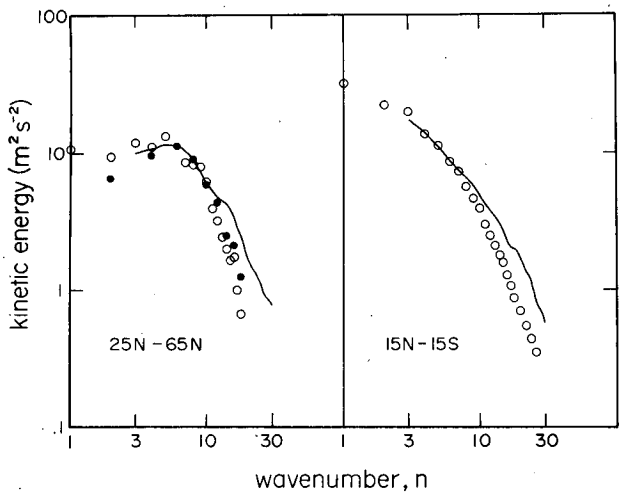

FIG. 5. The average of the cloud brightness spectra in Fig. 4 compared with eddy kinetic energy observations for midlatitudes (a) and the tropics (b). In (a) the open circles indicate eddy kinetic energies based on observed winds at 200 mb, 53°N (Julian and Cline, 1974), while the filled circles represent an average of results for 200, 500 and 850 mb at 40°N and 500 mb at 30 and 50°N using balanced winds over a 180 longitude interval (Julian *et al.*, 1970). The latter data are normalized to match the former at $n = 6$. In (b) the open circles correspond to a determination using observed winds at 200 mb, 10°N (Julian *et al.*, 1970). For both latitude regions, the cloud brightness power spectrum has been normalized to fit the observations at $n = 6$.

line for the average of the IR images alone. Note that there is no curve for the 15°N–15°S region for the GOES image since there is data only from 10–58°N, and that the Mariner 10 image spectra begin at wavenumber 5 because of the 92° phase angle (cf. Table 2). While there is significant variability among the spectra for each zone, the difference in the behavior at low wavenumbers between the midlatitude and equatorial regions is apparent. Three of the spectra for the midlatitude zone have a maximum in the wavenumber 5–7 region, and the fourth exhibits a definite flattening for wavenumbers <10. In contrast, the spectra for the equatorial zone show no indication of such a peak.

The difference between the two latitude zones is quite evident in Fig. 5, in which the solid lines represent the average of the respective power spectra from all of the Earth images. Fig. 5a compares that average for the midlatitude zone with observed eddy kinetic energy data indicated by the open and filled circles. The open circles represent eddy kinetic energies derived from observed winds for June–August 1970–71 at the 200 mb level, 53°N by Julian and Cline (1974), while the filled circles correspond to an average of the energy spectra obtained by Julian *et al.* (1970) for 200, 500 and 850 mb at 40°N and 500 mb at 30 and 50°N, using balanced winds for July–August 1963–67 over a 180° longitude interval. The latter values are normalized to fit the former at wavenumber 6, which is the same procedure employed in the vertical positioning of the brightness distribution power spectrum. Observed eddy kinetic energy representing the tropics and shown in Fig. 5b by the open circles is that determined by Julian *et al.* (1970) from streamline-isotach analyses of observed winds for March–August 1968 at 200 mb, 10°N. The corresponding equatorial zone average power spectrum from the Earth images is again normalized to match the eddy kinetic energy at wavenumber 6.

Examination of the results of other determinations of the eddy kinetic energy spectra for midlatitude regions reveals that the data shown in Fig. 5 are in fact typical, in the sense that they display two characteristic features: 1) there is a maximum in the kinetic energy near wavenumber 5 or 6, or at least an obvious flattening of the spectrum for wavenumbers $\lesssim 8$; and 2) the slope in the region of wavenumbers 8–20 is on the order of -2.5–3. Some seasonal dependence is noted, with the kinetic energy somewhat higher at all wavenumbers during winter. Also, slightly lower relative values for wavenumbers 1–3 during summer tend to emphasize the peak in the kinetic energy near wavenumber 5 or 6. The Southern Hemisphere spectra derived by Price (1975) and Desbois (1975) show features similar to those in the Northern Hemisphere.

It is generally accepted (cf. Saltzman, 1970) that the peak near $n=6$ in the midlatitude kinetic energy spectrum corresponds approximately to the wavelength of maximum baroclinic amplification (Kuo, 1952). The slope for wavenumbers larger than those in this region in which energy is injected is quite different from the $-5/3$ Kolmogoroff spectrum for the inertial subrange of three-dimensional homogeneous isotropic turbulence. It has therefore been suggested that the large-scale eddy motions correspond to a two-dimensional turbulence for which enstrophy rather than energy cascades to the higher wavenumbers, leading to a -3 power law (Kraichnan, 1967; Leith, 1968). This theory of two-dimensional turbulence also predicts a transfer of kinetic energy to wavenumbers lower than those at which the energy is injected. Although observational studies of the nonlinear exchange of energy and enstrophy tend to confirm some aspects of this picture, Steinberg *et al.* (1971) find that the evidence for the existence of an internal subrange in the 8–15 wavenumber region is inconclusive. Charney (1971) argues that in view of the importance of baroclinic processes, the assumption of a two-dimensional character for the atmospheric eddy motions is questionable. He finds, however, that the quasi-geostrophic nature of the flow in fact leads to a -3 power law by virtue of the conservation of pseudo-potential vorticity.

In contrast to the kinetic energy spectrum for midlatitudes, the observations for the equatorial region show no evidence of a peak or even a flattening near wavenumber 5 or 6. This is apparently consistent with the absence of the baroclinic conversion that is dominant in midlatitudes along with the importance of ultra-long waves of wavenumbers 1 and 2 as energy sources in the tropics (Kanamitsu *et al.*, 1972). The slope of the

equatorial spectrum for wavenumbers $\gtrsim 8$ is somewhat less steep than that for the midlatitudes, possibly the manifestation of a much different cascade process. In particular, Kanamitsu *et al.* (1972) find that wavenumbers 4–15 all receive energy from the zonal flow, and that there is a cascade of energy from wavenumbers 1 and 2 to larger wavenumbers.

Fig. 5 illustrates that the brightness distribution power spectra of the Earth images do reasonably well represent the major features of the kinetic energy spectra. The image spectrum for midlatitudes exhibits a very obvious peak in the wavenumber 5 to 6 region, whereas no such peak is evident for the equatorial zone; both results are clearly in agreement with the respective kinetic energy spectra. There is a general tendency for the cloud brightness spectra to show somewhat less steep slopes than those of the kinetic energy spectra for large wavenumbers. We estimate slopes of -1.6 for $7 \leqslant n \leqslant 15$ and -2.7 for $15 \leqslant n \leqslant 20$ from the midlatitude image spectrum, while the values for the kinetic energy data appear to be -2.0 and -3.1, respectively. For the equatorial region, we find slopes of -1.1 for $3 \leqslant n \leqslant 7$ and -1.5 for $7 \leqslant n \leqslant 15$, compared to -1.2 and -2.0, respectively, for the kinetic energy spectrum. The qualitative agreement between image spectra and kinetic energy spectra appears to be particularly good if we restrict comparison to $n \lesssim 10$, perhaps indicating that terrestrial cloud clusters serve as markers most effectively for larger planetary-scale motions. While this comparison of course does not demonstrate that the two types of spectra for Venus should be similar, it suggests that such an assumption is reasonable.

If we compare the Venus image spectra shown in Fig. 3 with the results for the Earth (Fig. 5), similarities as well as distinguishing features are noted. The Venus spectrum for 35–55°S is actually quite similar to that for the equatorial region of the Earth, each exhibiting a slope less steep than -2 and with no indication of a peak for $n \geqslant 3$. While we find a definite peak near wavenumber 5 or 6 for the midlatitude Earth spectrum, the only hint of such a feature in the Venus spectra is a flattening of the equatorial zone spectrum at wavenumbers 3 and 4. The spectra for both planets show an easily discernible latitudinal variation, and for the Earth the variation agrees qualitatively with differences in the corresponding eddy kinetic energy spectra, as shown above.

4. Implications of the Venus image spectra

Fundamental to a meaningful interpretation of the Venus cloud brightness spectra is the question of what atmospheric level is thus being characterized. The essential features of the vertical structure of the main, white cloud deck, assumed to be a diffuse haze of concentrated sulfuric acid particles, appear to be specified with a reasonable degree of confidence. Cloud optical depth unity is at a pressure level near 50 mb ($\sim$68 km), with a particle number density of approximately 30 cm^{-3} (Kawabata and Hansen, 1975); the cloud base is apparently at an altitude between 30 and 50 km (Lacis, 1975; Marov and Moroz, 1976); and the cloud particle scale height is probably $\frac{1}{2}$–$\frac{2}{3}$ that of the gas scale height above 55 km (Lacis, 1975). However, pure concentrated sulfuric acid has no absorption in the blue and near ultraviolet and thus by itself cannot produce the lower albedo and contrasts observed in that part of the spectrum. Since the identity and mechanism for production of the requisite unknown absorber is at present speculative, its location and hence the level corresponding to the UV cloud features is obviously somewhat uncertain.

Elemental sulfur has been proposed as a candidate for the UV absorber by Prinn (1975) and Hapke and Nelson (1975), the latter suggesting that some of the sulfur must be incompletely polymerized in order to obtain the observed wavelength dependence of the Venus reflectivity. Young (1977) has argued that simple elemental sulfur can in fact explain in a natural way the variation with wavelength of the average contrast level and the spherical albedo by virtue of the large temperature dependence of the absorption edge near 400 nm for sulfur. He proposes a model in which the dark UV markings are caused by a cloud of large ($\sim$10 μm) elemental sulfur particles with its base near 35 km and with a variable penetration into the white sulfuric acid cloud up to altitudes as high as 64 km. Thus, the variability in the level of contrast over the disk for a particular wavelength is attributed to horizontal variation in the altitude of the top of the sulfur cloud, and hence different optical thicknesses of the conservatively scattering sulfuric acid cloud above the absorbing material. If this model of the Venus clouds should prove to be essentially correct, then the UV images correspond to a sampling of the region between about 58 and 68 km. We note, however, that regardless of the model adopted or the identity of the absorber, the darkest UV features typically observed may lie no deeper than optical depth $\sim$3 in a conservatively scattering sulfuric acid cloud (Lacis, 1975). Therefore, in spite of the speculative nature of our present understanding, it appears that the Venus cloud brightness spectra characterize a region of the atmosphere extending no deeper than $\sim$60 km.

It is known from radio occultation studies, Venera entry probe measurements and observations of the infrared thermal emission from the cloud tops that there is an adiabatic region in the Venus atmosphere extending from an altitude of 55–60 km down to at least 45 km and that a large, nearly isothermal region exists above about 60 km (Tomasko *et al.*, 1977). Thus, the clouds observed in the UV images apparently lie in a zone analogous to the tropopause and lower stratosphere in the terrestrial atmosphere. Because of the high static stability, there is a strong possibility that the dynamics

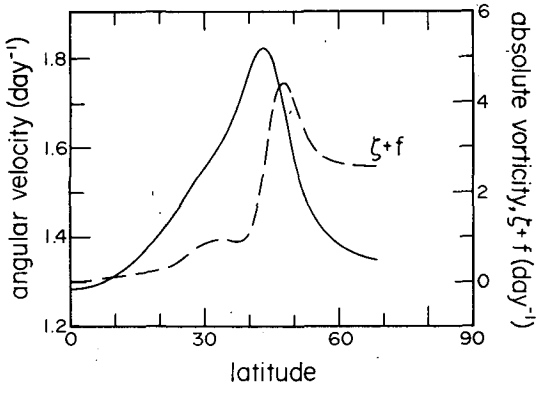

FIG. 6. Meridional profiles for the angular velocity of the mean zonal wind (solid line) and the absolute vorticity (dashed line) based on cloud-tracked wind determinations using the eight Mariner 10 images analyzed herein.

in this region can be characterized as barotropic, or two-dimensional (cf. Rossow and Williams, 1977).

Large-scale eddy motions corresponding to two-dimensional turbulence should display a -3 power spectrum for the eddy kinetic energy at wavenumbers larger than those in the region in which energy is injected (Kraichnan, 1967; Leith, 1968). The Venus cloud brightness spectrum for the equatorial region in fact exhibits a slope for wavenumbers larger than 5 of approximately -2.7 (cf. Fig. 3), a value remarkably close to -3 considering the typical result obtained in comparing observed eddy kinetic energy spectra for the Earth's atmosphere with the theoretically expected slope. It is therefore difficult to resist suggesting that the image power spectra do indeed characterize the eddy kinetic energy spectrum in the equatorial region, and that kinetic energy is apparently generated at wavenumbers less than 4 with larger wavenumbers constituting an inertial subrange for two-dimensional large-scale turbulence. We propose no mechanism responsible for the injection of kinetic energy at the lowest wavenumbers, but it is interesting to note that Dollfus (1975) found evidence for three semi-permanent features aligned along the equator in a synthesis of ground-based images, and Belton *et al.* (1976b) have associated a Kelvin wave, zonal wavenumber 1, in the equatorial region with the dark horizontal Y marking.

Clearly, the situation must be quite different in the midlatitude region, where we found the cloud brightness spectra to be characterized by a slope of -1.7—-2. Although the argument for two-dimensional turbulence based on the high static stability should in principle apply equally well to the midlatitude regions, there is independent evidence which suggests that another phenomenon plays an important role. Limaye and Suomi (1977) raised the question of whether the large meridional shear in the mean zonal wind near 45° latitude, as determined from tracking cloud motions (Suomi, 1975), might meet the necessary condition for barotropic instability. This has been considered also by Elson (1977) and Rossow and Williams (1977), and the latter, using a high-resolution numerical model, find that "solely as a consequence of the slow rotation, all zonal flows except solid body rotation and all planetary-scale waves with wavenumber greater than about two are barotropically unstable."

In order to examine in detail the possible importance of barotropic instability in understanding the midlatitude spectra, we have determined the meridional profile of the mean zonal wind for the eight Mariner 10 images under consideration by means of a cloud-tracked wind determination similar to that employed by Suomi (1975.)[5] Fig. 6 shows the resulting variation with latitude for the angular velocity of the mean zonal wind (solid line) as well as the absolute vorticity (dashed line) corresponding to that meridional profile. For a slowly rotating planet such as Venus, the effect of the Coriolis force is greatly reduced, while the curvature terms in the equations of motion become much more important. Consequently, it is the shear in the angular velocity which characterizes the tendency for instability, and the absolute vorticity should be evaluated in the spherical coordinate system. The necessary condition for barotropic instability is that an extremum in the absolute vorticity must exist in the region under consideration (cf. Kuo, 1951). The absolute vorticity relation in Fig. 6 illustrates that this condition is very definitely met at a latitude near 48° and possibly also at 33° and 37°.[6]

Using the specific meridional profile for the angular velocity thus derived for the eight images, we have obtained numerical solutions for the eigenvalue problem corresponding to the standard linearized perturbation treatment of the vorticity equation (cf. Kuo, 1951). Unstable barotropic perturbations are accordingly characterized by an angular phase velocity μ_r and a growth rate $n\mu_i$ for a disturbance of longitudinal wavenumber n. The results for the most unstable mode as a function of wavenumber are displayed in Fig. 7, where the growth rate is indicated by the solid line and the angular phase velocity is represented by the dashed line. It should be noted that the feature in the vorticity curve which results in critical points near 33° and 37° does not have a significant influence on the

[5] The mean profile is based on zonal averages using 2659 individual wind determinations covering latitudes from 70°S–35°N from four image pairs: FDS 63903 and 64117, 64747 and 64897, 65179 and 65473, 66223 and 66385. When profiles were calculated separately for the four pairs, no systematic differences were noted.

[6] We note that Suomi (1975) suggested that the meridional profile of the zonal wind might be consistent with conservation of angular momentum from the equatorial region to near latitude 45° and constant angular velocity poleward of that point. Our results indicate a region starting at approximately 43° where the zonal wind decreases more rapidly than the cosine of latitude in the poleward direction. It is this more rapid decrease which produces the peak in the angular velocity profile and the absolute vorticity extremum poleward of that peak.

solution for the most unstable models. Sensitivity studies using slightly different meridional velocity profiles showed that this feature is easily removed without affecting the principal amplified disturbances. Thus, it is the critical point near 48° that is responsible for the basic features of Fig. 7.

Although one is interested only in integral wavenumbers in practice, the computations were performed for non-integral values as well in order to allow smooth curves to be drawn. We note that there are two "families" of unstable disturbances, one between wavenumbers 1 and 3.7 with a nearly constant angular phase velocity and a maximum growth rate of about 0.06 day^{-1}, and the more unstable region between wavenumbers 3.4 and 11.4 with a maximum growth rate of more than 0.25 day^{-1} near $n = 7$. A more extensive description of these calculations and the results will be presented elsewhere.

Fig. 8 shows the relative kinetic energy as a function of latitude for the most unstable barotropic disturbance at wavenumber 7. A maximum at 47° is apparent, with an order of magnitude decrease by latitudes 34 and 57°. This behavior is quite similar to that at other wavenumbers, even those in the family of disturbances between $n=1$ and 3.7. Thus, barotropic instabilities consistent with the observed zonal flow appear to be localized in a zone remarkably coincident with that arbitrarily selected as characterizing the midlatitudes for the cloud brightness spectra. It therefore seems quite plausible that barotropic instabilities may in fact be responsible for the significant differences between the image power spectra for the midlatitude and equatorial regions.

We may speculate that the reason that the barotropic disturbances could produce a spectrum with a slope less steep than -3 is as follows. From Fig. 7 it is apparent that a band between wavenumbers 5 and 9 should be the

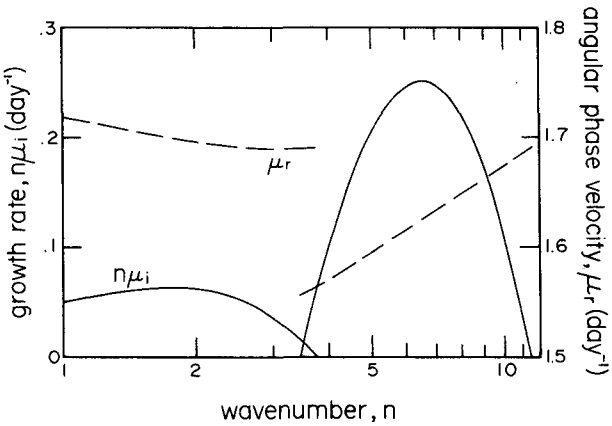

FIG. 7. Growth rate (solid line) and angular phase velocity (dashed line) for the most unstable barotropic disturbance at each wavenumber. These results are numerical solutions for the linearized perturbation vorticity equation in which we have used the specific meridional profile for the angular velocity of the mean zonal wind shown in Fig. 6.

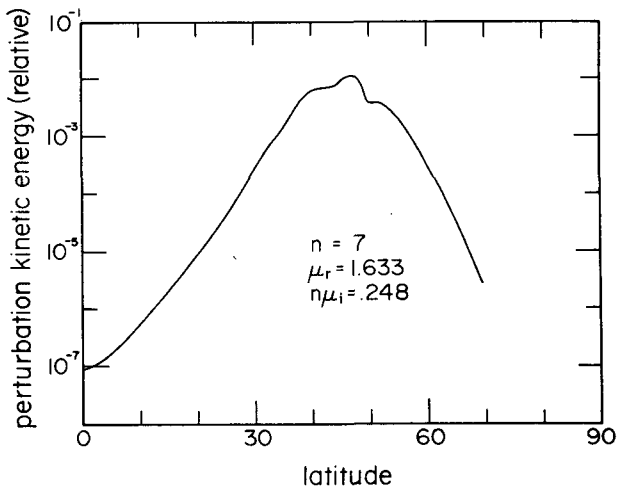

FIG. 8. Relative kinetic energy of the most unstable barotropic disturbances at $n = 7$ as a function of latitude.

principal region in which eddies gain energy (for amplified disturbances) at the expense of the mean zonal flow. Under the conditions of two-dimensional large-scale turbulence, there is a red cascade of energy to wavenumbers lower than those in the band in which energy is injected; and the eddy kinetic energy should exhibit a $-5/3$ power law in such an inertial subrange (Kraichnan, 1967). Since there are actually unstable modes at all wavenumbers between 1 and 11, there is probably no true inertial subrange, and the resulting slope might be expected to be intermediate to the $-5/3$ and -3 theoretical values. For wavenumbers >11, two-dimensional turbulence theory predicts another inertial subrange with cascading enstrophy and a -3 power law for the kinetic energy spectrum. Although the cloud brightness spectrum for the 35–55° latitude zone indicates no such change in slope at larger wavenumbers, we note that in the comparison with observed eddy kinetic energy for the terrestrial atmosphere, the image power spectra showed poorer agreement for wavenumbers $\gtrsim 10$.

If eddies are actually important relative to the mean meridional circulation, then the fact that the band of wavenumbers corresponding to maximum barotropic instability extends to near $n=10$ has important implications regarding numerical circulation models for the Venus atmosphere. Specifically, such models would apparently need a resolution sufficient to properly treat scales as small as 4000 km in the lower stratosphere and tropopause region.

5. Summary

Power spectrum analysis of Mariner 10 images for planetary zonal wavenumbers $n \gtrsim 3$ and for latitudes from 55°S–25°N yields spectra which show a systematic and apparently significant variation with latitude. Accordingly, average spectra were determined for three

latitude zones: an equatorial region from 15°N–15°S, a midlatitude region between 35 and 55°S, and the intermediate zone from 15–35°S. The spectrum for the equatorial region fits an approximately -2.7 power law for wavenumbers >5. In contrast, the midlatitude spectrum exhibits a slope of about -1.8 for $n \gtrsim 3$.

A comparison of the results for Venus with brightness distribution spectra for terrestrial clouds reveals similarities between the Venus midlatitude region spectrum and that for the equatorial region of the Earth. Although there is a well-defined peak near wavenumber 5 or 6 in the midlatitude spectrum for the Earth, the only indication of a departure from a general power law behavior for the Venus spectra is a flattening of the equatorial spectrum in the region of wavenumbers 3 and 4.

The results of a comparison between observed eddy kinetic energy and cloud brightness distribution spectra for the Earth lend support to the assumption that the two types of spectra should be correlated. The characteristics of the Venus image spectra consequently appear to be compatible with the interpretation that the observable clouds lie in a region of high static stability with the inertial eddy motions corresponding to two-dimensional turbulence. For the equatorial region it appears that the energy input must be at the very largest scales ($n < 4$), and we thus expect a spectrum with slope near -3 for larger wavenumbers. In the midlatitude zone, however, there is evidence that barotropic instability plays an important role and is responsible for the less steep slope observed in the image power spectra.

The fact that the observed mean zonal flow is barotropically unstable in midlatitudes is of course independent from the analysis of the cloud brightness spectra. However, unless it is simply a coincidence, the difference between the spectra in the equatorial and midlatitude regions is noteworthy in that it indicates that barotropic disturbances are not only possible, but that such eddies may be an important component in the atmospheric energy cycle and transports in the midlatitudes. Finally, there is the suggestion that it may be necessary to explicitly consider scales as small as wavenumber 10 in numerical investigations of the dynamics of this part of the Venus atmosphere.

Acknowledgments. I thank Dr. P. Stone for valuable discussions and suggestions. It is also a pleasure to acknowledge Dr. G. E. Danielson of the Image Processing Laboratory at the Jet Propulsion Laboratory for providing the Mariner 10 images. The GOES and SMS Earth images were kindly provided by Dr. S. Limaye. A microfiche catalog of Mariner 10 images and SEDR data on microfilm were made available by the National Space Science Data Center. I also thank Drs. Stone and J. Hansen for comments on the manuscript.

REFERENCES

Ainsworth, J. E., and J. R. Herman, 1975: Venus wind and temperature structure: The Venera 8 data. *J. Geophys. Res.*, **80**, 173–179.

——, and ——, 1977: On the reality of the Venus winds. *Icarus*, **30**, 314–319.

Antsibor, N. M., R. V. Bakit'ko, A. L. Ginzburg, V. T. Guslyakov, V. V. Kerzhanovich, Yu. F. Makarov, M. Ya. Marov, E. P. Molotov, V. I. Rogal'skii, M. K. Rozhdestvenskii, V. P. Sopokin and Yu. N. Shnygin, 1976: Estimates of wind velocity and turbulence from relayed Doppler measurements of the velocity of instruments dropped from Venera 9 and Venera 10. *Kosmich. Issled.*, **14**, 714–721.

Belton, M. J. S., G. R. Smith, D. A. Elliott, K. Klaasen and G. E. Danielson, 1976a: Space-time relationships in the UV markings on Venus. *J. Atmos. Sci.*, **33**, 1383–1393.

——, ——, G. Schubert and A. D. Del Genio, 1976b: Cloud patterns, waves, and convection in the Venus atmosphere. *J. Atmos. Sci.*, **33**, 1394–1417.

Boyer, C., and H. Camichel, 1961: Observations photographiques de la planète Venus. *Ann. Astrophys.*, **24**, 531–535.

——, and P. Guerin, 1969: Étude de la rotation retrograde, en 4 jours, de la couche exterieur nuageuse de Venus. *Icarus*, **11**, 338–355.

Chang, C. P., 1970: Westward propagating cloud patterns in the tropical Pacific as seen from time-composite satellite photographs. *J. Atmos. Sci.*, **27**, 133–138.

Charney, J. G., 1971: Geostrophic turbulence. *J. Atmos. Sci.*, **28**, 1087–1095.

Desbois, M., 1975: Large-scale kinetic energy spectra from Eulerian analysis of Éole wind data. *J. Atmos. Sci.*, **32**, 1838–1847.

Dollfus, A., 1975: Venus: Evolution of the upper atmospheric clouds. *J. Atmos. Sci.*, **32**, 1060–1070.

Elson, L., 1977: An atmospheric instability mechanism on a non-rotating planet and its application to Venus. *Bull. Amer. Astron. Soc.*, **9**, 508–509.

Gruber, A., 1974: The wavenumber-frequency spectra of satellite-measured brightness in the tropics. *J. Atmos. Sci.*, **31**, 1675–1680.

Hansen, J. E., and J. W. Hovenier, 1974: Interpretation of the polarization of Venus. *J. Atmos. Sci.*, **31**, 1137–1160.

Hapke, B., and R. Nelson, 1975: Evidence for an elemental sulfur component of the clouds from Venus spectrophotometry. *J. Atmos. Sci.*, **32**, 1212–1218.

Holloway, J. L. Jr., 1958: Smoothing and filtering of time series and space fields. *Advances in Geophysics*, H. E. Landsberg and J. Van Mieghem, Eds., Academic Press, 351–389.

Irvine, W. M., T. Simon, D. H. Menzel, J. Charon, G. Lecomte, P. Griboval and A. T. Young, 1968a: Multicolor photoelectric photometry of the brighter planets. II. Observations from Le Houga Observatory. *Astron. J.*, **73**, 251–264.

——, ——, ——, C. Pikoos and A. T. Young, 1968b: Multicolor photoelectric photometry of the brighter planets. III. Observations from Boyden Observatory. *Astron. J.* **73**, 807–828.

Julian, P. R., and A. K. Cline, 1974: The direct estimation of spatial wavenumber spectra of atmospheric variables. *J. Atmos. Sci.*, **31**, 1526–1539.

——, W. M. Washington, L. Hembree and C. Ridley, 1970: On the spectral distribution of large-scale atmospheric kinetic energy. *J. Atmos. Sci.*, **27**, 376–387.

Kanamitsu, M., T. N. Krishnamurti and C. Depradine, 1972: On scale interactions in the tropics during northern summer. *J. Atmos. Sci.*, **29**, 698–706.

Kawabata, K., and J. E. Hansen, 1975: Interpretation of the variation of polarization over the disk of Venus. *J. Atmos. Sci.*, **32**, 1133–1139.

Kerzhanovich, V. V., and M. Ya. Marov, 1977: On the wind velocity measurements from Venera spacecraft data. *Icarus*, **30**, 320–325.

Kraichnan, R. H., 1967: Inertial ranges in two-dimensional turbulence. *Phys. Fluids*, **10**, 1417–1423.

Kuo, H.-L., 1951: Dynamical aspects of the general circulation and the stability of zonal flow. *Tellus*, **3**, 268–284.

——, 1952: Three-dimensional disturbances in a baroclinic zonal current. *J. Meteor.*, **9**, 260–278.

Lacis, A. A., 1975: Cloud structure and heating rates in the atmosphere of Venus. *J. Atmos. Sci.*, **32**, 1107–1124.

Leith, C. E., 1968: Diffusion approximation for two-dimensional turbulence. *Phys. Fluids*. **11**, 671–673.

Limaye, S., and V. Suomi, 1977: A normalized view of Venus. *J. Atmos. Sci.*, **34**, 205–215.

Marov, M. Ya., and V. I. Moroz, 1976: Preliminary results of studies performed with space probes Venera 9 and Venera 10. *Kosmich. Issled.*, **14**, 651–654.

——, V. S. Avduevsky, V. V. Kerzhanovich, M. K. Rozhdestvensky, N. F. Borodin and O. L. Ryabov, 1973: Venera 8: Measurements of temperature, pressure and wind velocity on the illuminated side of Venus. *J. Atmos. Sci.*, **30**, 1210–1214.

Murray, B. C., M. J. S. Belton, G. E. Danielson, M. E. Davies, D. Gault, B. Hapke, B. O'Leary, R. Strom, V. Suomi and N. Trask, 1974: Venus: Atmospheric motion and structure from Mariner 10 pictures. *Science*, **183**, 1307–1315.

Price, P. G., 1975: A comparison between available potential and kinetic energy estimates for the Southern and Northern Hemispheres. *Tellus*, **27**, 443–452.

Prinn, R. G., 1975: Venus: Chemical and dynamical processes in the stratosphere and mesosphere. *J. Atmos. Sci.*, **32**, 1237–1247.

Reed, R. J., and E. E. Recker, 1971: Structure and properties of synoptic-scale wave disturbances in the equatorial western Pacific. *J. Atmos. Sci.*, **28**, 1117–1133.

Rossow, W. B., and G. P. Williams, 1977: A forced barotropic model as an analog of the stratosphere of Venus. *Bull. Amer. Astron. Soc.*, **9**, 508.

Saltzman, B., 1970: Large-scale atmospheric energetics in the wavenumber domain. *Rev. Geophys. Space Phys.*, **8**, 289–302.

Sato, M., K. Kawabata and J. E. Hansen, 1977: A fast invariant imbedding method for multiple scattering calculations and an application to equivalent widths of CO_2 lines on Venus. *Astrophys. J.*, **216**, 947–962.

Scott, A. H., and E. J. Reese, 1972: Venus: Atmospheric rotation. *Icarus*, **17**, 589–601.

Sikdar, D. N., J. A. Young and V. E. Suomi, 1972: Time-spectral characteristics of large-scale cloud systems in the tropical Pacific. *J. Atmos. Sci.*, **29**, 229–239.

Smith, B. A., 1967: Rotation of Venus: Continuing contradictions. *Science*, **158**, 114–116.

Steinberg, H. L., A. Wiin-Nielsen and C.-H. Yang, 1971: On nonlinear cascades in large-scale atmospheric flow. *J. Geophys. Res.*, **76**, 8629–8640.

Suomi, V., 1975: Cloud motions on Venus. *The Atmosphere of Venus*, J. Hansen, Ed., Goddard Institute for Space Studies, NASA SP-382, 42–58.

Tanaka, H., and O. Ryuguji, 1971: Spectrum analysis of tropical cloudiness (I). *J. Meteor. Soc. Japan*, **49**, 13–19.

——, and ——, 1973: Spectrum analysis of tropical cloudiness (II). *J. Meteor. Soc. Japan*, **51**, 93–100.

Tomasko, M. G., R. Boese, A. P. Ingersoll, A. A. Lacis, S. S. Limaye, J. B. Pollack, A. Sieff, A. I. Stewart, V. E. Suomi and F. W. Taylor, 1977: The thermal balance of the atmosphere of Venus. *Space Sci. Rev.*, **20**, 389–412.

Traub, W. A., and N. P. Carleton, 1975: Spectroscopic observations of winds on Venus. *J. Atmos. Sci.*, **32**, 1045–1059.

Travis, L. D., 1975: On the origin of ultraviolet contrasts on Venus. *J. Atmos. Sci.*, **32**, 1190–1200.

Wallace, J. M., 1970: Time-longitude sections of tropical cloudiness (December 1966–November 1967). ESSA Tech. Rep. NESC 56, Washington, DC, 37 pp.

——, 1971: Spectral studies of tropospheric wave disturbances in the tropical western Pacific. *Rev. Geophys. Space Phys.*, **9**, 557–612.

Young, A. T., 1977: An improved Venus cloud model. *Icarus*, **32**, 1–26.

Young, J. A., and D. N. Sikdar, 1973: A filtered view of fluctuating cloud patterns in the tropical Pacific *J. Atmos. Sci.*, **30**, 392–407.

Zangvil, A., 1975: Temporal and spatial behavior of large-scale disturbances in tropical cloudiness deduced from satellite brightness data. *Mon. Wea. Rev.*, **103**, 904–920.